Electronic Supplementary Material (ESI) for Journal of Materials Chemistry A.

Supporting Information

1D N-Doped Hierarchically Porous Hollow Carbon Tubes Derived from Supramolecular Template as Metal-Free Electrocatalysts for Highly Efficient Oxygen Reduction Reaction

Lei Zhao, [a] Xu-Lei Sui, [a] Qing-Yan Zhou, [a] Jia-Zhan Li, [a] Jing-Jia Zhang, [a] Guo-Sheng Huang, [b] Zhen-Bo Wang, [a,*]

[a] MIIT Key Laboratory of Critical Materials Technology for New Energy Conversion and Storage, School of Chemistry and Chemical Engineering, Harbin Institute of Technology, No. 92 West-Da Zhi Street, Harbin, 150001 China

[b] State Key Laboratory for Marine Corrosion and Protection, Luoyang Ship Material Research Institute (LSMRI), No. 149-1 Zhuzhou Road, Qingdao, 266101, P. R. China

* Corresponding author. Tel.: +86-451-86417853; Fax: +86-451-86418616.

Email: wangzhb@hit.edu.cn (Z.B. Wang)

Experimental Section

Preparation of MC supramolecular aggregate: Melamine cyanurate (MC) complex was prepared by a typical supramolecular self-assembling between cyanuric acid and melamine through three hydrogen bonds. An equimolar ratio of melamine and cyanuric acid were dissolved in 100 mL deionized water under strong agitation at 80 ^{o}C to initiate self-assembly. The obtained white precipitate was collected via filtration, washed with deionized water, and dried at 60 °C to get the melamine cyanurate supramolecular aggregate.

Preparation of h-NCTs: In a typical synthesis, 500 mg MC precursor was added into an aqueous solution of glucose (1 g glucose in 30 mL water) under sonication and stirring process. Then the resultant suspension was subjected to a 50 mL Teflon autoclave, and kept under hydrothermal condition at 160 °C for 10 h. A brown product collected through centrifugation, washed with deionized water, and dried overnight was labeled as MC@Glu. The final product h-NCTs were obtained by calcination of MC@Glu at different temperature under Ar atmosphere. h-NCTs products prepared at the calcination temperature of 800, 900, 1000 °C were labeled as h-NCT-800, h-NCT-900, and h-NCT-1000, respectively.

Characterization: The morphology of the samples was investigated by using scanning electron microscopy (SEM, Hitachi S4800), transmission electron microscope (TEM, FEI Tecnai G2 F20), and high-resolution transmission electron microscope (HRTEM, FEI Tecnai G2 F20). The structure and composition of samples were scrutinized by Powder X-ray diffraction (XRD, Rigaku D/max-RB diffractometer), Raman spectra (Raman, Renishaw1000) and X-ray photoelectron spectroscopy (XPS, PHI model 5700 instrument). XPS analysis was carried out with a physical electronics PHI model 5700 instrument. The Al X-ray source was

operated at 250 W and the take-off angle of the sample to analyzer was 45°. Survey spectra were collected at pass energy (PE) of 187.85 eV over a binding energy range from 0 eV to 1300 eV. High binding energy resolution multiplex data for the individual elements were collected at a PE of 29.55 eV. During all XPS experiments, the pressure inside the vacuum system was maintained at 1×10^{-9} Pa. Before the analysis above, all the samples were dried under vacuum at 80°C overnight. The binding energies were calibrated based on the graphite C 1s peak at 284.625 eV. Intensities were estimated by calculating the integral of each peak, after smoothing, subtraction of the Shirley-shaped background, and fitting the experimental curve to a combination of Lorentzian and Gaussian peak shape. The specific surface area and pore size distributions were determined by nitrogen adsorption–desorption isotherms according to the Brunauer-Emmett-Teller (BET) method using a QUADRASORB SI analyzer.

Electrochemical tests: The catalyst ink was prepared as follows: 5 mg of h-NCTs catalyst and 25 μL of Nafion solution (5 wt%) were added to 2 mL of ethanol under sonication for 30 min. Then 15μL of the resulting catalyst ink was cast onto a pre-polished glassy carbon rotating disk electrode (RDE) or rotating ring-disk electrode (RRDE) and dried at room temperature. Commercial Pt/C catalyst (20 wt%, E-TEK) was used as a benchmark for comparison. RDE/RRDE covered with prepared catalyst served as the working electrode. A platinum wire and Ag/AgCl electrode served as the counter and reference electrodes. The potentials of the reference electrode were calibrated with respect to reversible hydrogen electrode (RHE) performed in the high purity hydrogen saturated electrolyte. All the potentials were reported with respect to RHE. All electrochemical measurements were performed in a three-electrode system on an electrochemical workstation (CHI 760E, CH

Instrument, China). Electrochemical measurements including cyclic voltammetry, linear sweep voltammetry and durability test were carried out in an O_2 saturated 0.1 mol L^{-1} KOH and 0.5 M H_2SO_4 aqueous solution at room temperature. The tolerance of catalyst to methanol cross-over was conducted with chronoamperometric measurement by quickly injecting of methanol into 0.1 mol L^{-1} KOH electrolyte to reach a concentration of 1 mol L^{-1} at ≈ 200 s.

The K–L plots (I^{-1}vs $\omega^{-1/2}$) were obtained according to linear fitting of the reciprocal rotating speed versus reciprocal current density at various electrode potentials. The electron transfer number during ORR was calculated by Koutecky-Levich equation:

$$\frac{1}{I} = \frac{1}{I_K} + \frac{1}{I_D}$$

$$I_D = 0.62nFAD^{2/3}\omega^{1/2}v^{-1/6}C_{O2}$$

where I is the measured current density, I_K and I_D are the kinetic and diffusion-limiting current, respectively, n is transferred electron number, ω is the angular velocity, F is Faraday constant (96485 C mol^{-1}), C_{O2} is the bulk concentration of O_2 (1.2×10^{-6} mol cm^{-3}), A is the electrode area (0.246 cm^2), D is the diffusion coefficient of O_2 in 0.1 mol L^{-1} KOH (1.9×10^{-5} cm^2 s^{-1}), and v is the kinetic viscosity of the electrolyte (0.01 cm^2 s^{-1}).

RRDE measurements were carried out to determine the four-electron selectivity. The disk electrode was scanned at a rate of 5 mV s^{-1}. The electron transfer number and hydrogen peroxide yield (%H_2O_2) calculated from the RRDE measurement was according to following equation:

$$n = \frac{4I_D}{I_D + \frac{I_R}{N}}$$

$$H_2O_2\,\% = \frac{\frac{2I_R}{N}}{I_D + \frac{I_R}{N}} \times 100\%$$

where I_D and I_R are the disk and ring currents, respectively. N is the ring current collection efficiency which was determined to be ~37 %.

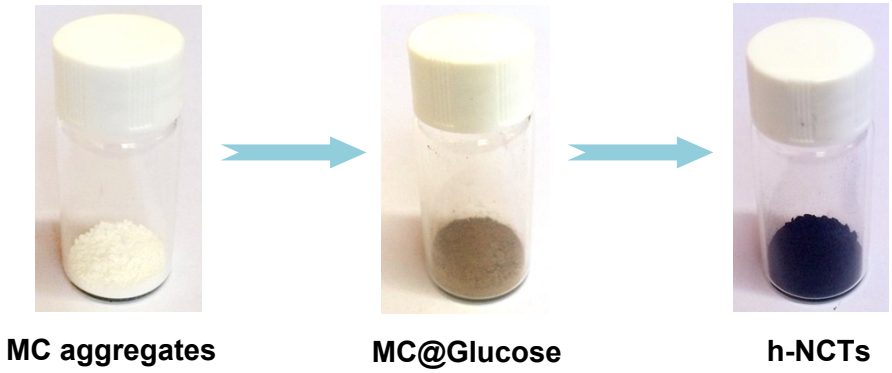

Figure S1. Photograph images of the MC supramolecular aggregates, MC@Glucose and h-NCTs sample powders with various colors.

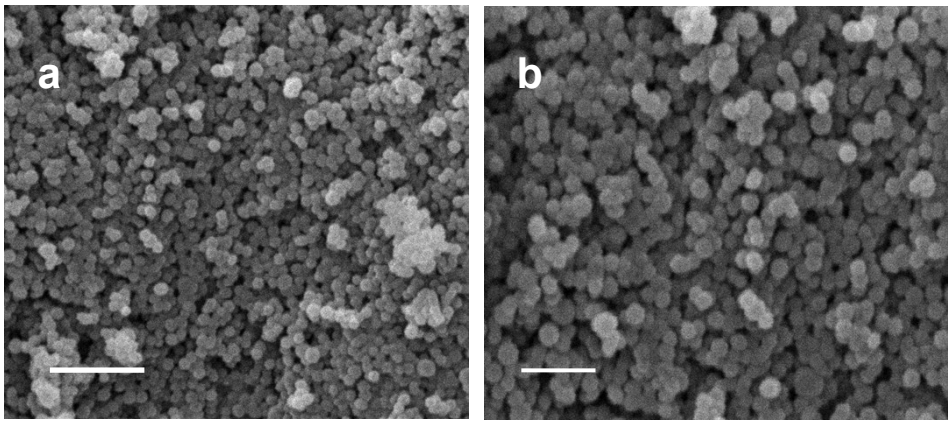

Figure S2. SEM images of carbon spheres derived from hydrothermal carbonization of glucose

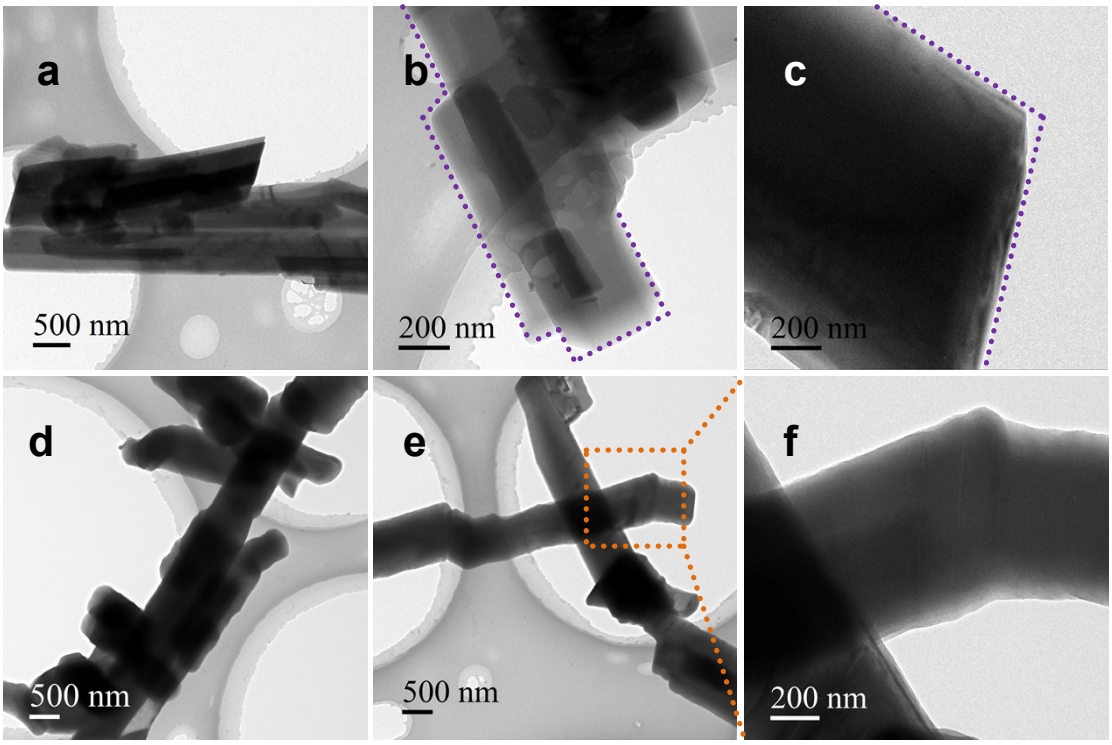

Figure S3. SEM images of MC aggregates (a-c) and MC@Glu (d-e)

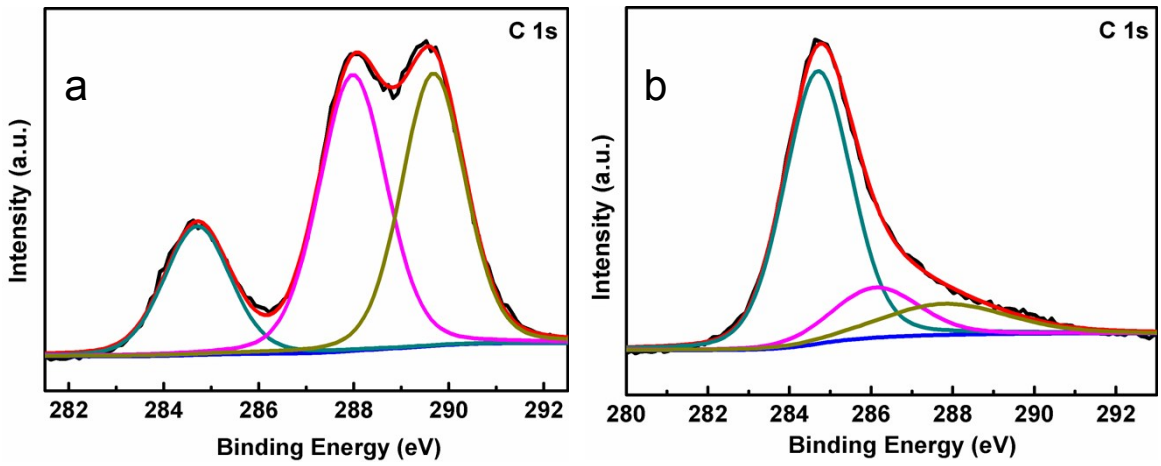

Figure S4. High resolution C 1s XPS spectrum of MC aggregate and MC@Glu.

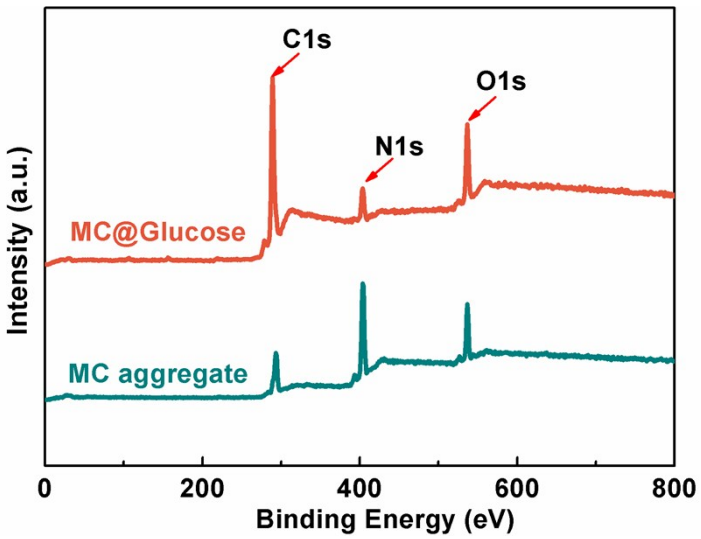

Figure S5. The full XPS spectrum of MC aggregate and MC@Glu.

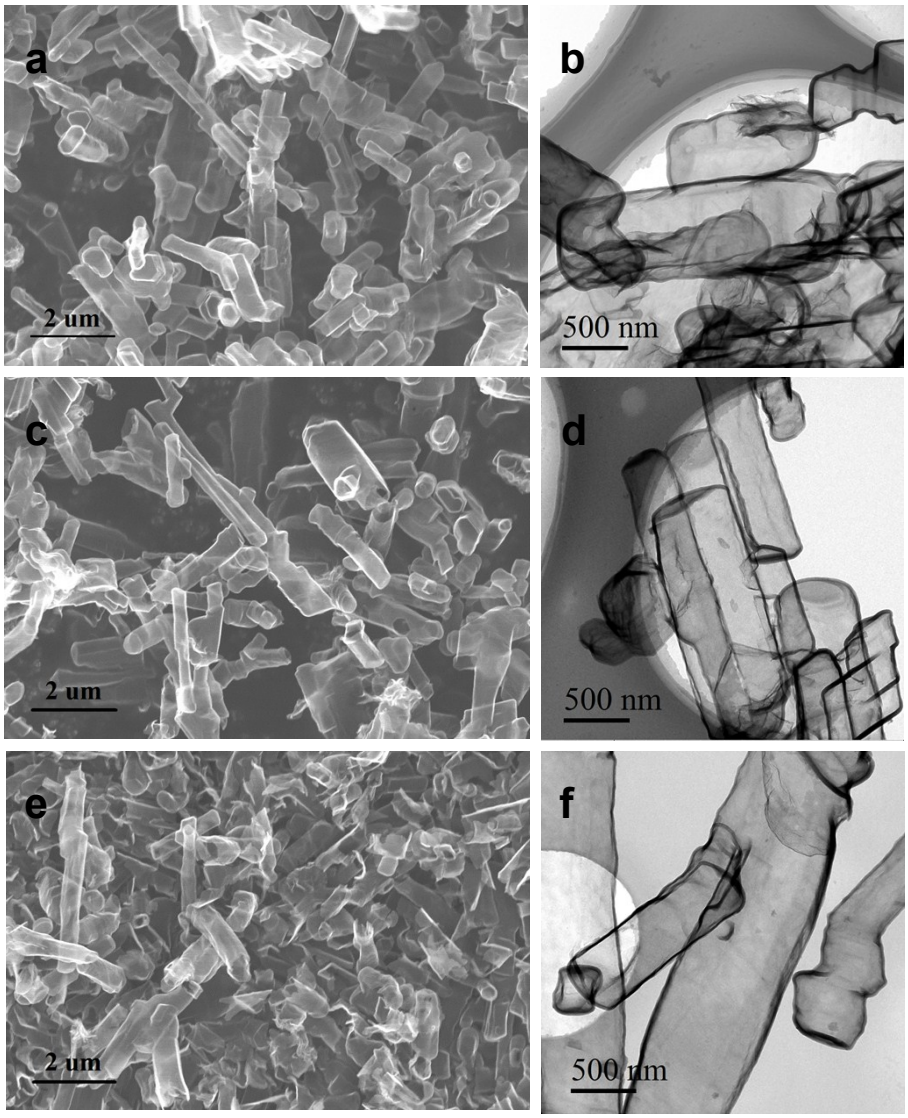

Figure S6. SEM and TEM images of h-NCT-800 (a, b), h-NCT-900 (c,d) and h-NCT-1000 (e, f).

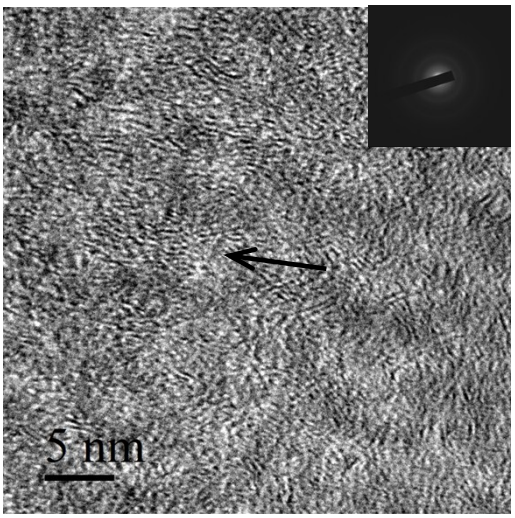

Figure S7. HRTEM image and corresponding SAED pattern of h-NCT-800 sample.

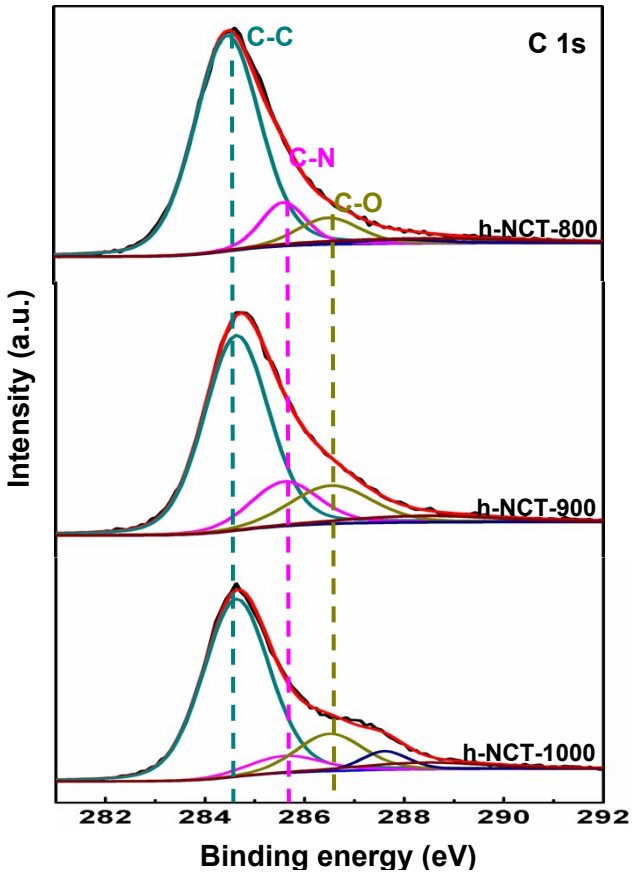

Figure S8. High resolution C 1s XPS spectrums of h-NCT-800, h-NCT-900 and h-NCT-1000.

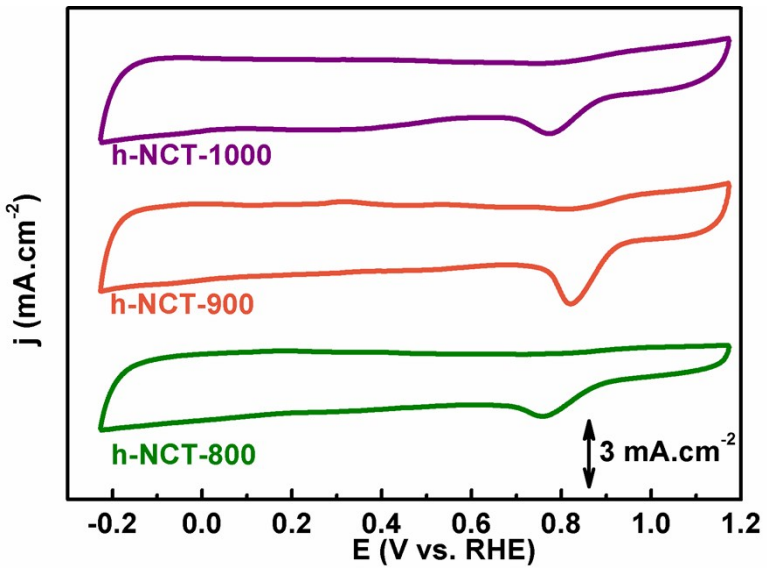

Figure S9. CV curves of h-NCT-800, h-NCT-900 and h-NCT-1000 in O_2 saturated 0.1 M KOH aqueous solution with a scan rate of 50 $mV \cdot s^{-1}$.

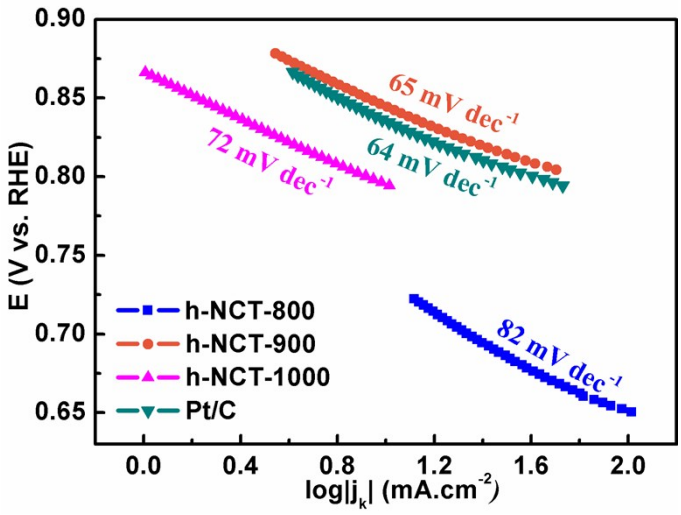

Figure S10. Tafel plots for h-NCT-800, h-NCT-900, h-NCT-1000 and commercial Pt/C catalysts derived from the LSVs.

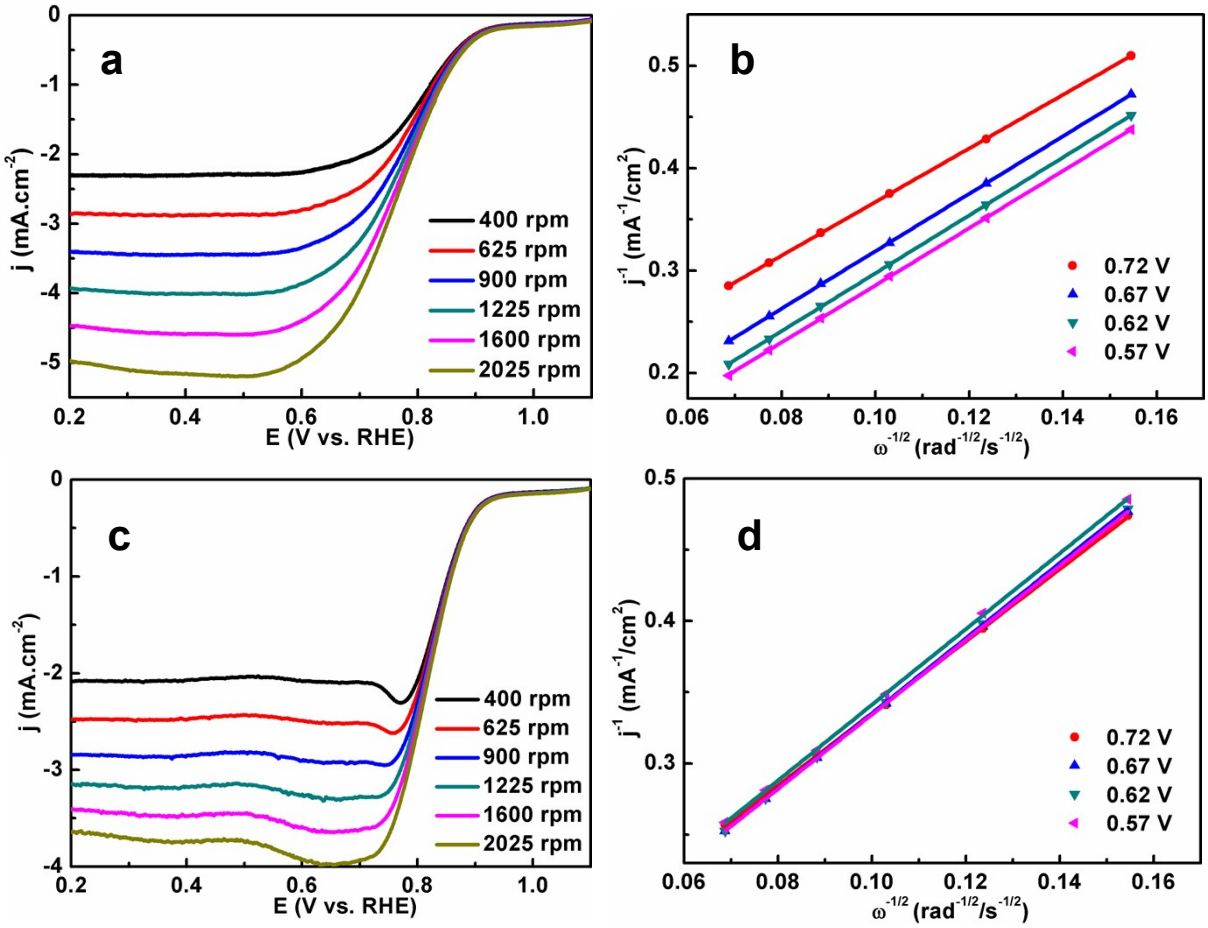

Figure S11. ORR polarization curves of h-NCT-800 (a, b) and h-NCT-1000 (c, d) in O_2-saturated 0.1 M KOH solution at different rotating speeds and its corresponding Koutecky–Levich plots.

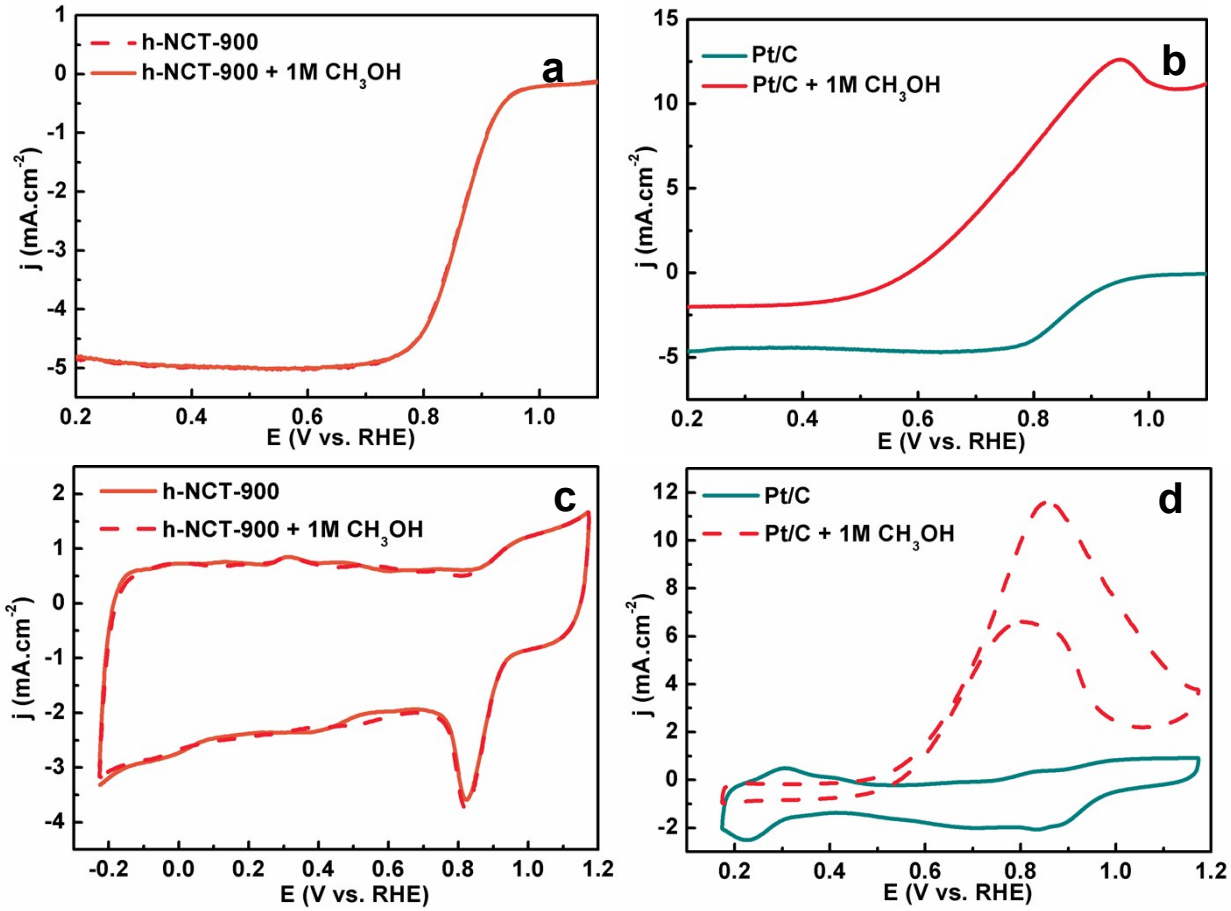

Figure S12. LSV (a, b) and CV (c, d) curves of h-NCT-900 and Pt/C catalysts in O_2-saturated 0.1 M KOH with and without 1 M MeOH.

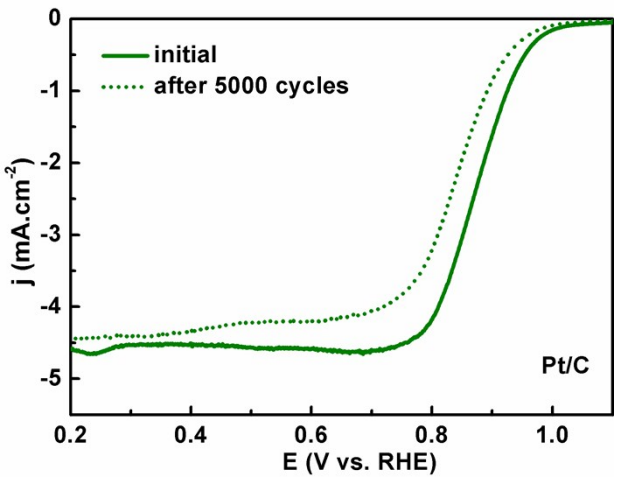

Figure S13. LSV curves of the commercial Pt/C catalysts in O_2-saturated 0.1M KOH solutions before and after durability test.

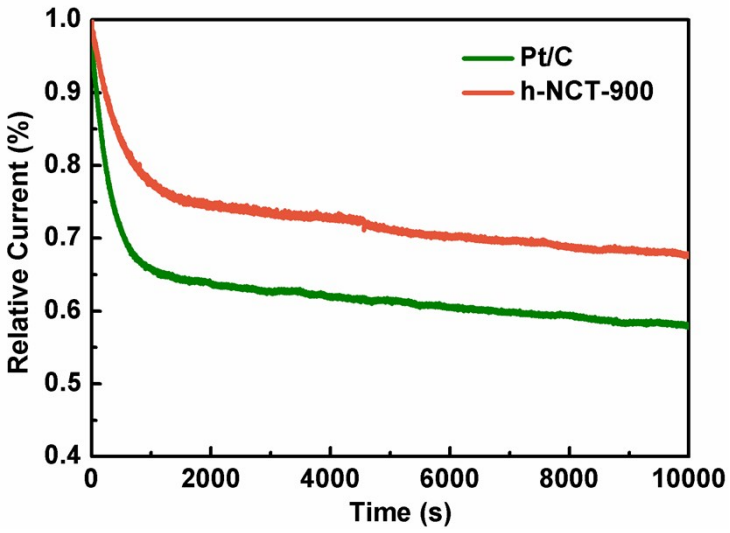

Figure S14. Chronoamperometric curves of h-NCT-900 and commercial Pt/C in O_2-saturated 0.1 mol L^{-1} KOH solution with rotating speed of 1600 rpm.

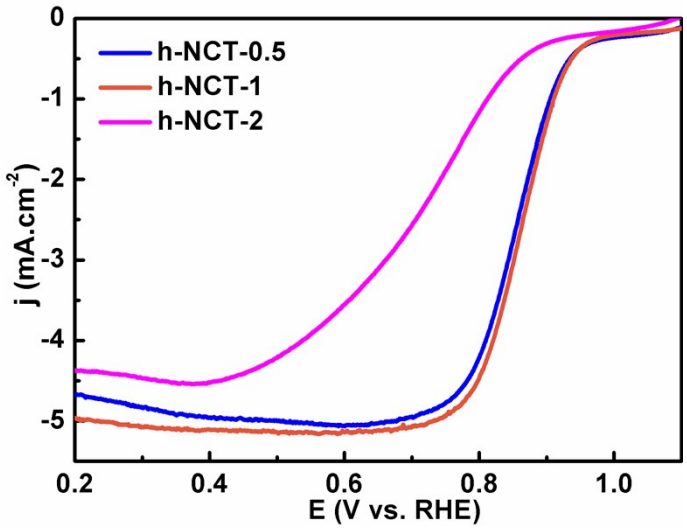

Figure S15. LSV curves of h-NCTs samples prepared with different amounts of glucose in O_2-saturated 0.1 M KOH electrolyte at a scanning rate of 10 mV s^{-1} with a rotating speed of 1600 rpm.

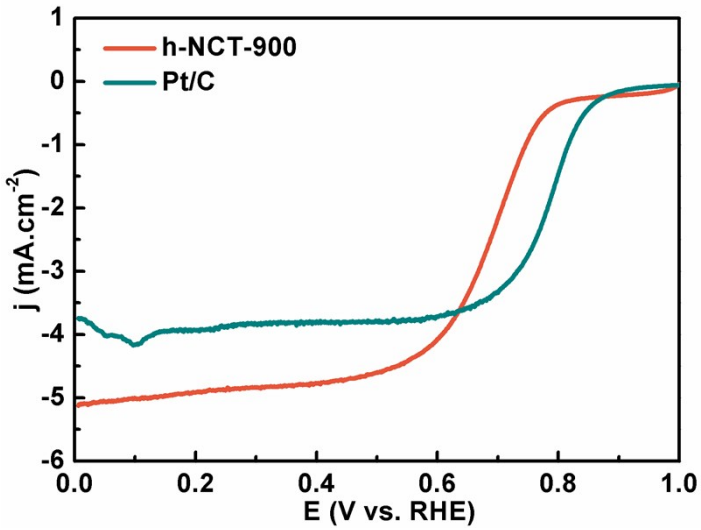

Figure S16. LSV curves of h-NCT-900 and commercial Pt/C in O_2-saturated 0.5 M H_2SO_4 electrolyte at a scanning rate of 10 mV s^{-1} with a rotating speed of 1600 rpm.

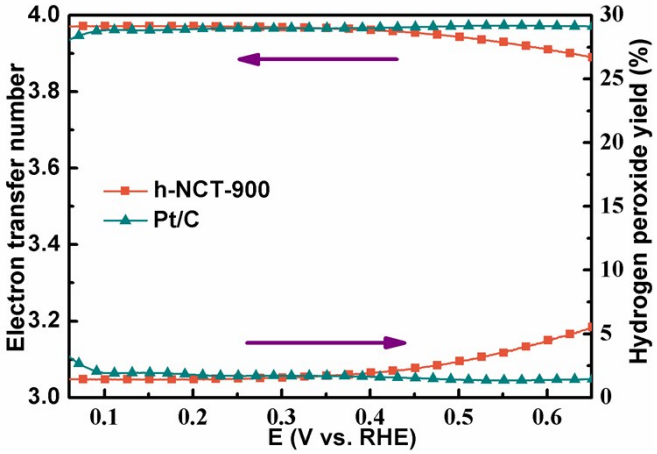

Figure S17. Peroxide yield and the calculated electron transfer number of h-NCT-900 and commercial Pt/C catalysts in O_2-saturated 0.1 M H_2SO_4 electrolyte.

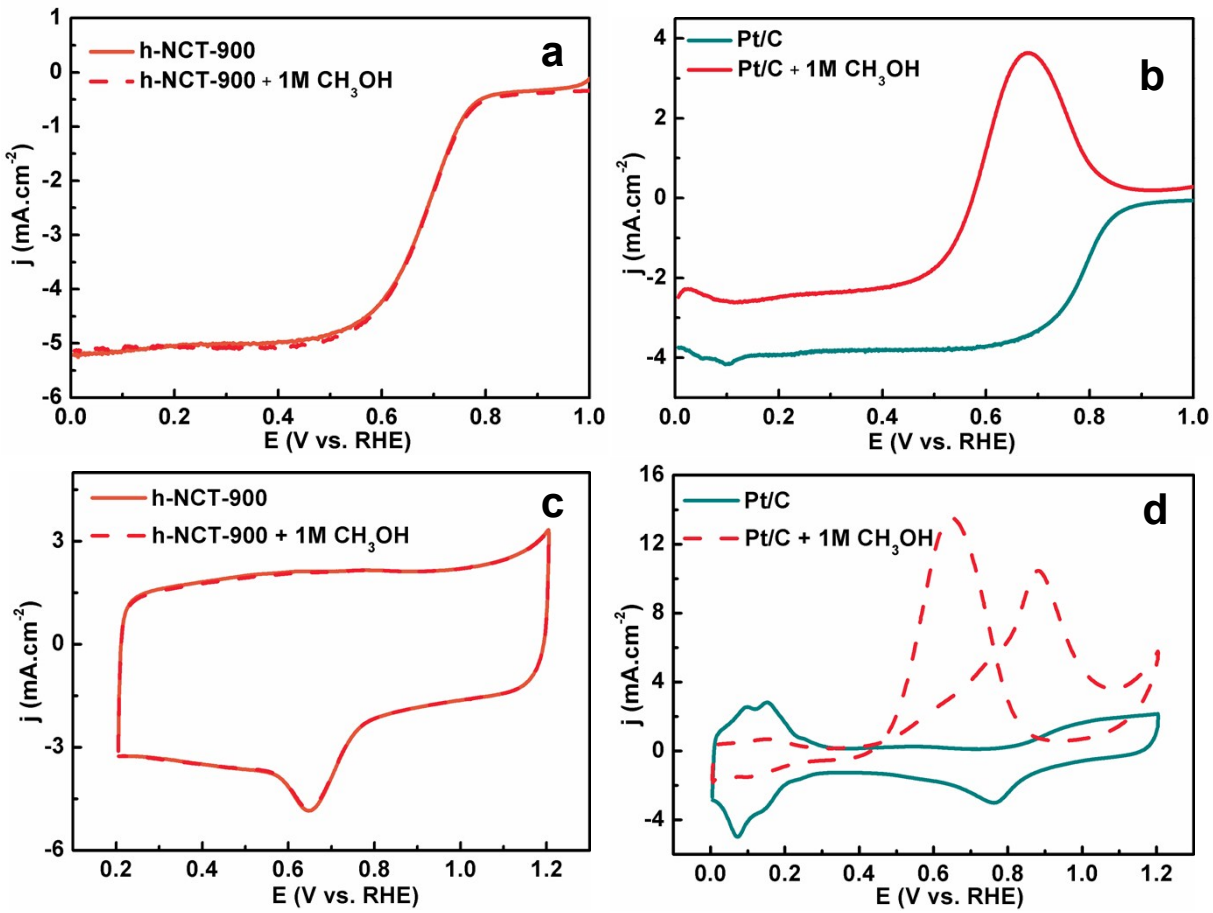

Figure S18. LSV (a, b) and CV (c, d) curves of h-NCT-900 and Pt/C catalysts in O_2-saturated 0.5 M H_2SO_4 with and without 1 M MeOH.

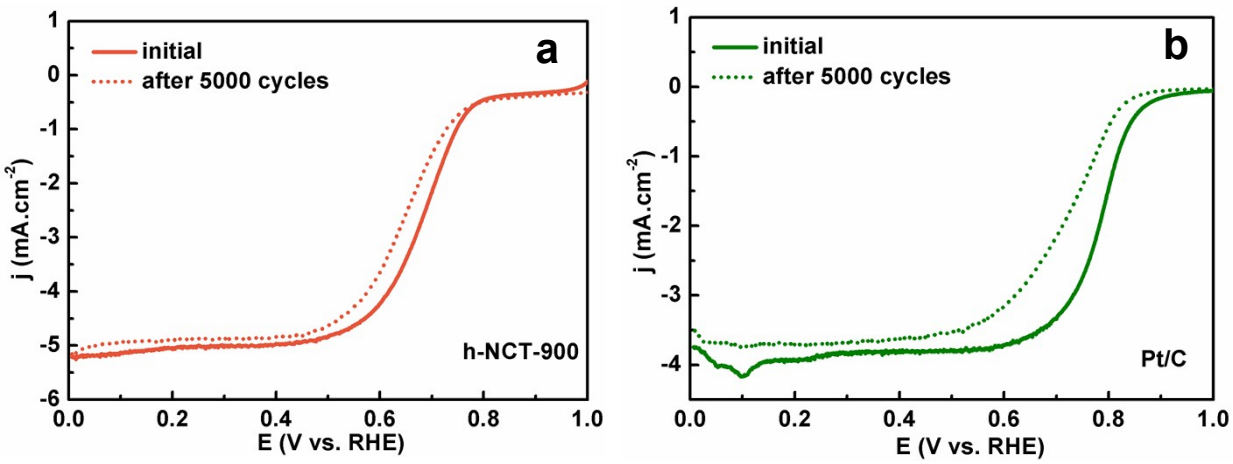

Figure S19. LSV curves of the h-NCT-900 (a) and commercial Pt/C (b) catalysts in O_2-saturated 0.5 M H_2SO_4 electrolyte before and after durability test.

Table S1. Comparison of ORR performance under alkaline conditions for our synthesized h-NCT-900 sample with other reported benchmark catalysts

catalyst	$E_{on\text{-}set}$ *vs. RHE / V*	$E_{1/2}$ *vs. RHE / V*	*reference*
N, P-doped CNT/graphene hybrid nanospheres	0.94	0.82	Gao_ Adv Mater_2016[1]
Nitrogen-doped carbon nanosheets	0.95	0.84	Feng_Angew. Chem. Int. Ed_2014[2]
N, S co-doped honeycomb carbon	0.87	0.74	Wang_ Adv Funct Mater_2016[3]
Nitrogen doped graphene derived by polypyrrole and graphene aerogel	0.92	0.74	Chen_ACS Appl Mater Interfaces_2015[4]
Nitrogen and sulfur co-doped carbon nanotube/graphene nanoribbon	0.97	0.81	Wang_J Mater Chem A_2016[5]
N,P-mesoporous nanocarbon	0.94	0.85	Dai_NatNanotech_2015[6]
N-doped hierarchically porous carbon	0.92	0.85	Feng_Nat Commun_2014[7]
Porous carbon nanofibers templated by Te nanowires	0.88	0.79	Yu_JACS_2014[8]
nitrogen-doped carbon nanosheets templated by C_3N_4	0.89	0.76	Zhang_ Adv Mater_2016[9]
foam-like $NiCo_2O_4$ derived by starch templating	0.82	0.63	Wu_Small_2016[10]
h-NCT-900	**0.97**	**0.86**	**this work**

Table S2. Comparison of ORR performance under acid conditions for our synthesized h-NCT-900 sample with other reported benchmark catalysts

catalyst	$E_{on\text{-}set}$ *vs. RHE / V*	$E_{1/2}$ *vs. RHE / V*	*reference*
N, P-doped CNT/graphene hybrid nanospheres	0.90	0.68	Gao_ Adv Mater_2016[1]
Nitrogen-doped carbon nanosheets	0.75	0.57	Feng_Angew. Chem. Int. Ed_2014[2]
N-doped arbon spheres	0.65	0.42	Lu_ Adv Mater_2014[11]
N,P-mesoporous nanocarbon	0.83	0.62	Dai_NatNanotech_2015[6]
N-doped hierarchically porous carbon	0.84	0.72	Feng_Nat Commun_2014[7]
N-doped mesoporous carbon derived from ionic liquids and nucleobases	0.8	0.5	Yang_JACS_2011[12]
Fe–N-doped carbon capsules	0.80	0.52	Titirici_ ACS Nano_2016[13]
Iron-coordinated nitrogen-doped carbon	0.82	0.6	Xu_JACS_2014[14]
Nitrogen-doped ordered mesoporous	0.80	0.60	Dai_Chem Mater_2010[15]
Mesoporous Fe-N-doped carbon nanofibers	0.84	0.62	Yu_Angew. Chem. Int. Ed_2015[16]
h-NCT-900	**0.85**	**0.68**	**this work**

References

1. J. Yang, H. Sun, H. Liang, H. Ji, L. Song, C. Gao and H. Xu, *Adv. Mater.*, 2016, **28**, 4606-4613.
2. W. Wei, H. Liang, K. Parvez, X. Zhuang, X. Feng and K. Müllen, *Angewandte Chemie*, 2014, **126**, 1596-1600.
3. W. Tian, H. Zhang, H. Sun, A. Suvorova, M. Saunders, M. Tade and S. Wang, *Adv. Funct. Mater.*, 2016, **26**, 8651-8661.
4. M. Wang, J. Wang, Y. Hou, D. Shi, D. Wexler, S. D. Poynton, R. C. T. Slade, W. Zhang, H. Liu and J. Chen, *ACS Appl. Mat. Interfaces*, 2015, **7**, 7066-7072.
5. J. Wang, Z. Wu, L. Han, R. Lin, W. Xiao, C. Xuan, H. L. Xin and D. Wang, *J. Mater. Chem. A*, 2016, **4**, 5678-5684.
6. J. Zhang, Z. Zhao, Z. Xia and L. Dai, *Nat Nano*, 2015, **10**, 444-452.

7. H.-W. Liang, X. Zhuang, S. Brüller, X. Feng and K. Müllen, *Nature communications*, 2014, **5**, 4973.
8. W. Zhang, Z.-Y. Wu, H.-L. Jiang and S.-H. Yu, *J. Am. Chem. Soc.*, 2014, **136**, 14385-14388.
9. H. Yu, L. Shang, T. Bian, R. Shi, G. I. N. Waterhouse, Y. Zhao, C. Zhou, L.-Z. Wu, C.-H. Tung and T. Zhang, *Adv. Mater.*, 2016, **28**, 5080-5086.
10. L. Liu, J. Wang, Y. Hou, J. Chen, H.-K. Liu, J. Wang and Y. Wu, *Small*, 2016, **12**, 602-611.
11. K. Ai, Y. Liu, C. Ruan, L. Lu and G. Lu, *Adv. Mater.*, 2013, **25**, 998-1003.
12. W. Yang, T.-P. Fellinger and M. Antonietti, *J. Am. Chem. Soc.*, 2011, **133**, 206-209.
13. G. A. Ferrero, K. Preuss, A. Marinovic, A. B. Jorge, N. Mansor, D. J. L. Brett, A. B. Fuertes, M. Sevilla and M.-M. Titirici, *Acs Nano*, 2016, **10**, 5922-5932.
14. L. Lin, Q. Zhu and A.-W. Xu, *J. Am. Chem. Soc.*, 2014, **136**, 11027-11033.
15. X. Wang, J. S. Lee, Q. Zhu, J. Liu, Y. Wang and S. Dai, *Chem. Mater.*, 2010, **22**, 2178-2180.
16. Z.-Y. Wu, X.-X. Xu, B.-C. Hu, H.-W. Liang, Y. Lin, L.-F. Chen and S.-H. Yu, *Angew. Chem. Int. Ed.*, 2015, **54**, 8179-8183.